

EXTINCTION AND DUST GEOMETRY IN M83 H II REGIONS: A HUBBLE SPACE TELESCOPE/WFC3 STUDY

GUILIN LIU^{1,2}, DANIELA CALZETTI¹, SUNGRYONG HONG^{1,3}, BRADLEY WHITMORE⁴, RUPALI CHANDAR⁵, ROBERT W. O'CONNELL⁶, WILLIAM P. BLAIR^{2,7}, SETH H. COHEN⁸, JAY A. FROGEL⁹ AND HWIHYUN KIM⁸

¹Astronomy Department, University of Massachusetts, Amherst, MA 01003, USA

²Center for Astrophysical Sciences, Johns Hopkins University, Baltimore, MD 21218, USA; liu@pha.jhu.edu

³National Optical Astronomy Observatory, Tucson, AZ 85719, USA

⁴Space Telescope Science Institute, Baltimore, MD 21218, USA

⁵Department of Physics and Astronomy, University of Toledo, Toledo, OH 43606, USA

⁶Astronomy Department, University of Virginia, P.O. Box 3818, Charlottesville, VA 22903, USA

⁷Visiting Astronomer, Las Campanas Observatory, La Serena, Chile

⁸School of Earth and Space Exploration, Arizona State University, Tempe, AZ 85287, USA and

⁹Galaxies Unlimited, Lutherville, MD 21093, USA

Accepted for publication in ApJ Letters 2013

ABSTRACT

We present HST/WFC3 narrow-band imaging of the starburst galaxy M83 targeting the hydrogen recombination lines ($H\beta$, $H\alpha$ and $Pa\beta$), which we use to investigate the dust extinction in the H II regions. We derive extinction maps with 6 parsec spatial resolution from two combinations of hydrogen lines ($H\alpha/H\beta$ and $H\alpha/Pa\beta$), and show that the longer wavelengths probe larger optical depths, with A_V values larger by $\gtrsim 1$ mag than those derived from the shorter wavelengths. This difference leads to a factor $\gtrsim 2$ discrepancy in the extinction-corrected $H\alpha$ luminosity, a significant effect when studying extragalactic H II regions. By comparing these observations to a series of simple models, we conclude that a large diversity of absorber/emitter geometric configurations can account for the data, implying a more complex physical structure than the classical foreground “dust screen” assumption. However, most data points are bracketed by the foreground screen and a model where dust and emitters are uniformly mixed. When averaged over large ($\gtrsim 100$ – 200 pc) scales, the extinction becomes consistent with a “dust screen”, suggesting that other geometries tend to be restricted to more local scales. Moreover, the extinction in any region can be described by a combination of the foreground screen and the uniform mixture model with weights of 1/3 and 2/3 in the center ($\lesssim 2$ kpc), respectively, and 2/3 and 1/3 for the rest of the disk. This simple prescription significantly improves the accuracy of the dust extinction corrections and can be especially useful for pixel-based analyses of galaxies similar to M83.

Subject headings: galaxies: individual (M83, NGC 5236) — galaxies: ISM — dust, extinction

1. INTRODUCTION

Interstellar dust attenuates and reddens the light from stars, by both absorbing and scattering it, producing what is termed “dust extinction”. When dealing with individual stars, one can usually assume that the dust (absorber) is located exclusively in front of the star (emitter) and is well separated from it, thus simplifying the treatment of dust extinction. The analysis of the light-attenuating effects of dust quickly becomes extremely complicated when extended sources, such as stellar populations, are the emitters, and absorbers and emitters can distribute to produce complex geometries. This is generally the case of external galaxies, where individual stars are unresolved; in this case we term “dust attenuation” the combined effects of extinction and geometry. The assumption that the absorbers are located in front of the emitters and well separated from them is widely applied in astronomy even for external galaxies, but is far from accurate.

Probing the actual geometry of the dust distribution in an external galaxy is a challenging task that requires multiple-band measurements across a wide range of the electromagnetic spectrum with very high spatial resolution. The hydrogen recombination emission lines provide a convenient tool, commonly used for deriving both the

dust extinction and the dust geometry. The intrinsic ratios of these lines are easily calculated theoretically, and show little variation for a wide range of physical and chemical conditions. For case B recombination, changes in the electron density of an H II region between 10^2 and 10^4 cm^{-3} and in the temperature between 5×10^3 and 10^4 K, the $H\alpha/H\beta$ line ratio only changes between 3.04 and 2.85 ($\sim 7\%$), and $H\alpha/Pa\beta$ between 16.5 and 17.6 (also $\sim 7\%$, Osterbrock & Ferland 2006; Dopita & Sutherland 2003). Case B recombination and the adopted density and temperature ranges are appropriate for most extragalactic nebulae. Observing two hydrogen lines yields a crude measurement of the foreground extinction (similar to what is done for individual stars), but at least three or more lines, ideally widely spaced in wavelength, are needed to constrain both extinction and geometry.

The starburst galaxy M83 has been imaged in multiple narrow bands targeting hydrogen recombination lines ($H\beta$ and $H\alpha$ in the optical, and $Pa\beta$ in the near-IR), as part of the Early Release Science (ERS) observations made by the HST/WFC3 Scientific Oversight Committee (SOC), which enables an unprecedented detailed study of the dust extinction and geometry in the nebular gas of a nearby galaxy.

M83 (NGC 5236, a.k.a. the “Southern Pin-

wheel Galaxy”), is classified as an SAB(s)c (de Vaucouleurs et al. 1991), is one of the closest grand design-spirals (4.56 Mpc), is virtually face-on, and has a starburst nucleus, a marked bar, and prominent spiral arms. These properties make it an ideal target for detailed investigations of dust extinction in extragalactic H II regions.

2. DATA PROCESSING

M83 was mapped with HST/WFC3 in 2009 August, with a series of narrow and broad band filters in the UVIS and IR channels, as part of the ERS program (GO-11360, PI: Robert O’Connell; see Chandar et al. 2010 for further details of the program and the full list of filters used to observe M83). The narrow-band filters included those in the H β (λ 4861Å, F487N), H α + [N II] (λ 6563Å+ λ 6548, 6584Å, F657N) and Pa β (λ 12818Å, F128N) emission lines. The observations cover two pointings: the southern pointing targets the nuclear region of M83 and about half of its northeastern arm, and the northern pointing targets an adjacent field of the same area where the southwestern arm winds over. The field of view (FoV) for each pointing subtends 3.6×3.6 kpc² for H α and H β , and 3.1×2.7 kpc² for Pa β .

The raw data were first processed with the *MultiDrizzle* software (Fruchter et al. 2009) to accomplish both basic and high-level processing, including flat-fielding, cosmic-ray cleaning, combination, mosaicing of the two pointings, and registration of all mosaics onto a common grid (Mutchler 2010).

We proceed at matching the point spread functions (PSFs) of the UVIS and IR channels. Direct measurements of point sources in the images yield PSFs with $0''.07$, $0''.07$ and $0''.22$ FWHM for H β , H α , and Pa β , respectively. We thus degrade the UVIS images ($0''.07$ resolution) to match the resolution of IR data ($0''.22$) by convolving the former to a Gaussian kernel. Finally, we resample the images from both channels (original pixel sizes are $0''.04$ for UVIS and $0''.13$ for IR) to a 7×7 grid of the original UVIS data, obtaining a final pixel size of $0''.28$ (6.1 pc).

To produce pure hydrogen emission line images, we subtract a rescaled F110W image from the F128N image to remove the stellar continuum. The stellar continuum images for H β and H α lines are determined by linearly interpolating between the F438W and F555W and between the F555W and F814W images, respectively. For each individual pointing in each line, we subtract the stellar continuum by matching the fluxes of a sample of stars, and then measure and remove the global background. Filter throughput corrections for the shifted lines at the 513 km s^{-1} heliocentric recession velocity of M83 (Koribalski et al. 2004) amount to only 1–3%. Each emission line image is also corrected for foreground Galactic extinction using the color excess value $E(B - V) = 0.066$ mag, as reported in NED¹.

The F657N filter allows [N II] λ 6548, 6584Å doublet, which needs to be removed to obtain the H α emission. To account for spatial variations in the [N II]/H α ratio, we

use the measurements in Bresolin & Kennicutt (2002), who have obtained spectroscopic data for 11 H II regions in the disk and 5 regions in the core of this galaxy. Our FoV covers 5 of the disk regions and all the nuclear regions. We assign the spectroscopic [N II]/H α ratio determinations to areas surrounding each H II region from the Bresolin & Kennicutt (2002) paper. Figure 1 shows the distribution of the adopted ratios, color coded in terms of the total $([\text{N II}]\lambda 6548\text{Å} + [\text{N II}]\lambda 6584\text{Å})/\text{H}\alpha$ ratio. For the areas outside the immediate surroundings of each H II region and for the entire northern pointing (which does not contain any H II region studied by Bresolin & Kennicutt 2002), we assume the value of Region 11 in their paper, the one closest to the average of the four regions located on the northeastern spiral arm.

3. RESULTS

For our galaxy with super-solar metallicity ($12 + \log [\text{O}/\text{H}] = 8.94$, Bresolin & Kennicutt 2002; Hong et al. 2013), we adopt an electron temperature $T_e = 7500$ K and a number density $n_e = 10^3 \text{ cm}^{-3}$ as the fiducial environment in the whole galaxy, implying intrinsic ratios $I_{\text{H}\alpha}/I_{\text{H}\beta} = 2.92$ and $I_{\text{H}\alpha}/I_{\text{Pa}\beta} = 17.1$ (Dopita & Sutherland 2003) (note that our results are not sensitive to the specific choice of the electron density or temperature, see Section 1). We adopt the extinction curve presented by Cardelli et al. (1989), with $k(\text{H}\alpha) = 2.535$, $k(\text{H}\beta) = 3.609$ and $k(\text{Pa}\beta) = 0.840$, in the expression $I_{\text{obs}}/I_{\text{intr}} = 10^{-0.4k(\lambda)E(B-V)}$. Two extinction maps are then created, one derived from the ratio of H α to H β and the other from that of H α to Pa β , as shown in Figure 2, using only pixels above the 5σ detection level in all three maps. Our main limitation is the depth of the H β line, which is the most dust attenuated one among the three.

3.1. Extinction and dust content

Figure 3 shows the histograms of A_V derived from the two line ratios. A significant number of pixels in the H α /H β ratio map have negative values of A_V , due to the large error bars (typically ~ 1 mag). In general, A_V from H α /H β shows a narrow distribution peaked at ~ 0.5 mag, while A_V from H α /Pa β shows a double peak at ~ 2 and ~ 5.5 mag. Rebinning our maps with a coarser grid hardly changes the shapes and the peak locations of the histograms (cf. the color lines in the figure). We also show these histograms in a series of galactic annuli, which clearly demonstrate that A_V (H α /Pa β) peaks at a larger value than A_V (H α /H β) in every annulus (also see Table 1), and the second peak of A_V (H α /Pa β) mentioned above is largely contributed by the nucleus, where many pixels with large and patchy dust attenuation are present (e.g., Thatte, Tezca, & Genzel 2000).

Although the size of dust grains spans a wide range, the extinction in V-band ($\lambda = 5500\text{Å}$) is dominated by the grains with a radius $a \sim \lambda/2\pi \sim 0.1 \mu\text{m}$, thus we can derive the dust column density using $A_V = 1.086 \tau_V = 1.086 \pi a^2 N_d$, and further calculate the dust mass by assuming the solid density of the grain material to be $\rho_d = 3 \text{ g cm}^{-3}$, a compromise between graphite and crystalline olivine (Draine 2011). Using A_V (H α /Pa β)

¹ <http://ned.ipac.caltech.edu>. The NASA/IPAC Extragalactic Database (NED) is operated by the Jet Propulsion Laboratory, California Institute of Technology, under contract with the National Aeronautics and Space Administration.

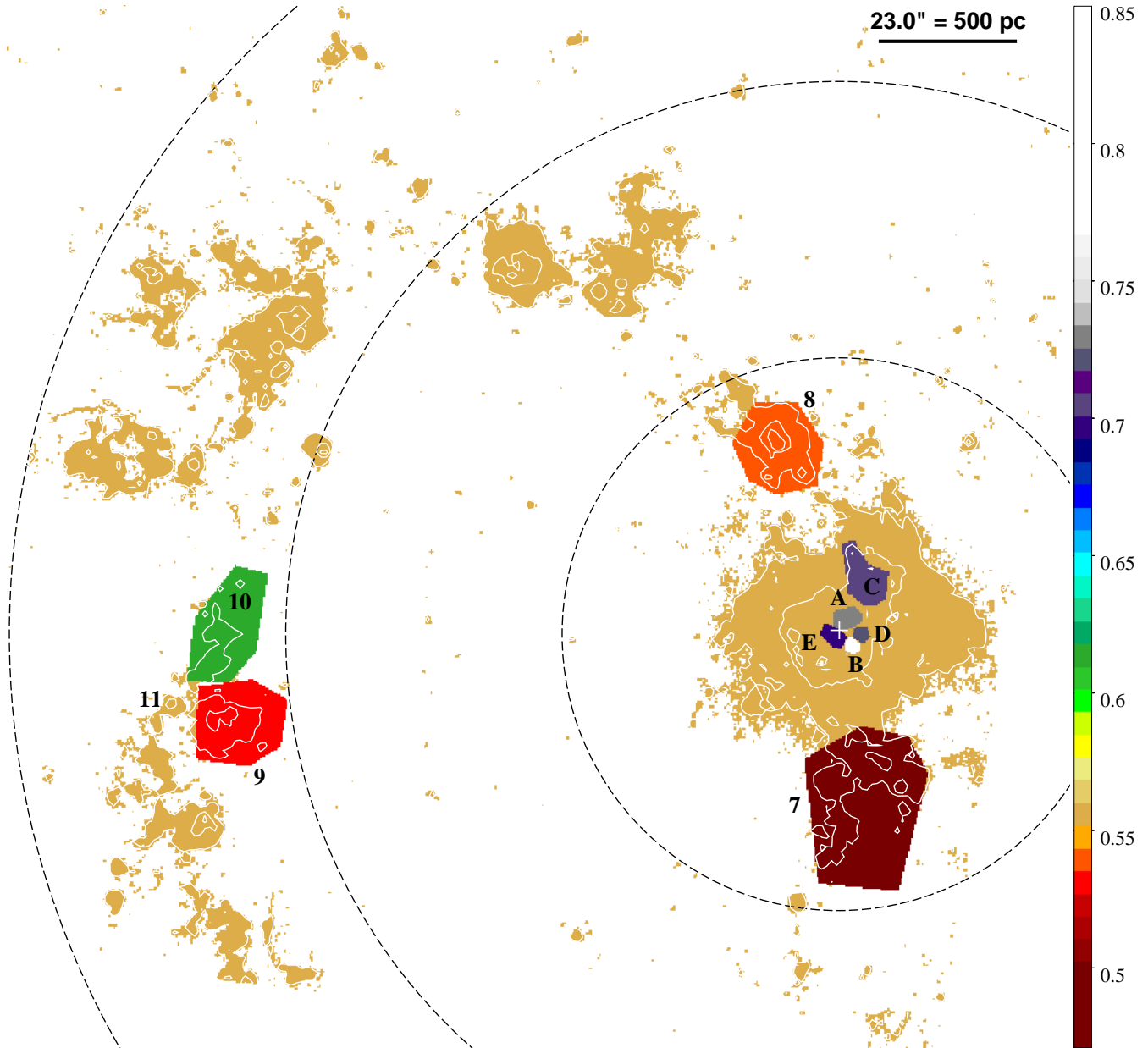


Figure 1. The $[\text{N II}]/\text{H}\alpha$ ratio map for M83 adopted in this work, overlaid on the $\text{H}\alpha + [\text{N II}]$ contour map. The letters and numbers denote the regions studied by Bresolin & Kennicutt (2002). Only the southern pointing is shown because none of the H II regions in the northern pointing has been observed by those authors. The color bar to the right indicates the ratio of the total intensity of the nitrogen doublet ($\lambda\lambda 6548, 6584\text{\AA}$) to the $\text{H}\alpha$ line intensity. The kinematic nucleus is marked with a white plus sign following Knapen et al. (2010), and the black dashed circles depict the galactic radii of 1, 2 and 3 kpc that are used for the calculations in Table 1 and Figure 3.

which is likely closer to the actual extinction than A_V ($\text{H}\alpha/\text{H}\beta$), we find the dust mass in the whole FoV to be $7 \times 10^5 M_\odot$. The entire galaxy has ~ 24 times of this amount ($\sim 2 \times 10^7 M_\odot$), as our FoV covers $\sim 8\%$ of the disk ($12.9' \times 11.5'$, NED), and a factor of 2 is to account for the dust in the excluded $\text{S/N} < 5$ regions. This estimation, although an upper limit (these faint regions likely do not contribute that much, and the galaxy center, the most dusty region, is covered by our FoV), is consistent with previous studies using infrared and (sub)millimeter data (Galametz et al. 2011 find $8.5 \times 10^6 M_\odot$; Foyle et al. 2012 find $4 \times 10^7 M_\odot$), and is similar to the dust content

of other metal-rich spiral galaxies (e.g., Liu et al. 2010; Draine et al. 2007).

3.2. Dust geometry

The availability of three hydrogen emission lines also enables a crude analysis of the dust geometry in the H II regions, by comparing the observationally derived extinction to models of the emitters/absorbers geometry. The simplest geometry, the foreground screen, in which the dust grains form a homogeneous, non-scattering screen foreground to the emitting light source, is such that any pair of hydrogen lines will yield the same A_V value. This is clearly not the case in M83. When the A_V values de-

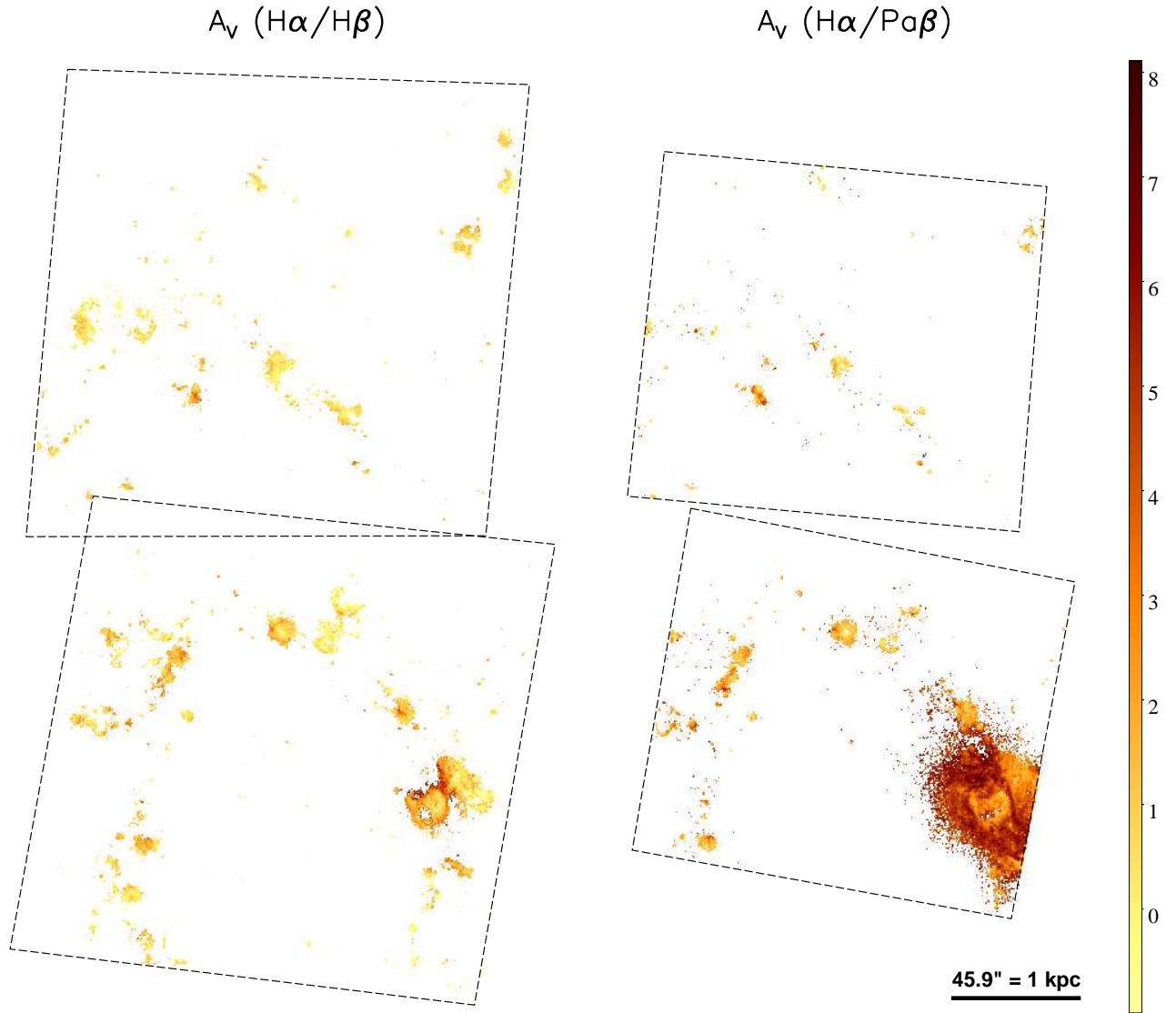


Figure 2. The visual extinction (A_V) maps in M83. These two A_V maps are derived from the $H\alpha/H\beta$ (left) and $H\alpha/P\alpha\beta$ (right) line ratios. The southern and northern pointings have been mosaiced, and the colorbar shows the value of A_V in magnitudes. The margins of the FoVs are depicted by the black dash lines for both the northern and the southern pointings.

Table 1
Derived dust properties in M83.

Region (1)	$A_V(\frac{H\alpha_{tot}}{H\beta_{tot}})$ (2)	$A_V(\frac{H\alpha_{tot}}{P\alpha\beta_{tot}})$ (3)	$\langle A_V(\frac{H\alpha}{H\beta}) \rangle$ (4)	$\langle A_V(\frac{H\alpha}{P\alpha\beta}) \rangle$ (5)	$\log(N_d)$ (6)
all	1.48	2.65	0.61	4.04	10.07
0–1 kpc	1.75	3.40	1.15	4.65	10.13
1–2 kpc	0.82	2.65	0.23	1.58	9.67
2–3 kpc	1.37	1.46	0.72	1.88	9.74
3–4 kpc	1.33	0.68	0.50	1.14	9.53
4–5 kpc	1.42	0.02	0.31	1.09	9.50

Note. — (1) Region for calculation. (2–3) Visual extinction derived from the ratio of the total line emission from the considered region (mag). (4–5) Median value of the A_V maps (i.e., Figure 2) within this region (mag). (6) Dust Column density converted from Column 5 (cm^{-2}). Note that the method for columns 4–6 is for high resolution studies, while the calculation for columns 2–3 is relevant for analyses where only coarse resolution images (e.g. those of distant galaxies) are available.

rived from $H\alpha/H\beta$ and from $H\alpha/Pa\beta$ are compared to each other, as shown in Figure 4, they do not follow a relation with a slope of unity, as expected in the case of the foreground screen. Instead, the data points are broadly distributed in the upper half of the diagram, delimited by the one-to-one line and the vertical $A_V = 0$ line.

In order to describe the behavior observed in Figure 4, we follow Calzetti et al. (1994) and Natta & Panagia (1984) and calculate the predictions of five simple models with plane-parallel absorber/emitter configurations (for a schematic representation of the models, see Calzetti et al. 1994):

1. The foreground screen model, as described above (no clumpiness and scattering is present, as the screen is uniform and physically distant from the light emitter).
2. The clumpy dust screen model. Like Natta & Panagia (1984) and Calzetti et al. (1994), we assume all the clumps to have the same optical depth and to be Poisson distributed, with an average of N clumps along the line of sight.
3. The uniform scattering slab model. In this case the dust is located close to the emitter and the scattering by the dust grains into the line of sight has an important positive contribution. We follow the calculation procedure of Calzetti et al. (1994), but with the physical parameters of the dust from Witt & Gordon (2000).
4. The clumpy scattering slab model. The properties of this model is a combination of models 2 and 3. Same dust parameters are used as in model 3. The same value of N as model 2 has been adopted.
5. The uniform mixture model. The dust and emitters are homogeneously mixed together, and the scattering into the line of sight is taken into account.

The relations between the visual extinction derived from these hydrogen lines predicted by the above models are shown in Figure 4. The average number of clumps in models 2 and 4 are set to be $N = 6$ in the figure. Model 5 has the interesting property that the tip of the line is the limit when the optical depth becomes infinitely large, in which case neither of the three emission lines can explore deep into the H II regions. None of the five models can, alone, account for the distribution of all data points, even when taking the fairly large error bars into account. The spread in extinction values is significant and spans the range covered by all 5 models. A significant number (30.4%) of regions with $A_V(H\alpha/H\beta) < 2$ mag have extinction values $A_V > 2$ mag when the latter is derived from $H\alpha/Pa\beta$. For these regions, the traditional use of the $H\alpha/H\beta$ line ratio to derive extinction values produces a significant underestimate of the intrinsic values, by factors >2 (up to ~ 10). This is in line with the conclusions of Israel & Kennicutt (1980) and Skillman & Israel (1988) that deriving dust extinction in H II regions at longer wavelengths results in larger values than at shorter wavelengths.

The extinction values are almost evenly distributed between the two extreme lines marked by models 1 and 5

(and even beyond those models), suggesting a large variation in the dust geometry among different H II regions. At the same time, these models clearly encompass the majority of the data, when the data uncertainties are taken into account. The envelope represented by model 1 and model 5 suggests that for most H II regions/nebulae, the uniform mixture and the foreground screen models bracket the range of absorber/emitter geometric configurations.

Although clearly an over-simplification of the complex dust geometry, model 1 represents 46% of the area of H II regions well (within 1/2 magnitude of extinction). The most deviant points are located in the nuclear regions of this galaxy.

Moreover, rebinning our maps onto a very coarse ($\gtrsim 20 \times 20$) grid significantly suppresses the necessity to introduce model 5. For instance, at a sampling scale of ~ 180 pc (30×30) all data points agree with a dust screen configuration (Figure 4). This is consistent with Kennicutt et al. (2009): when averaged over large sub-galactic regions, the mean extinction becomes consistent with the foreground dust screen model, suggesting that other geometries tend to be more localized.

4. POTENTIAL APPLICATIONS

In spite of the significant uncertainty of the derived A_V , the data points in Figure 4 appear to form two branches: one of which approximately follows the locus of model 5 (the “uniform mixture branch”), while the other favors models 1–4 whose degeneracy between each other is difficult to break and therefore can be represented by model 1 (the “foreground screen branch”). Projecting these two branches to the M83 images will provide an empirical prescription for extinction correction in spatially resolved galaxies.

These two branches can be reasonably divided by the straight line that bisects all the data points $A_V(H\alpha/Pa\beta) = 1.428 A_V(H\alpha/H\beta)$ (the blue line in Figure 4). To investigate the spatial distribution of the data points separated by this line, we calculate the ratio of the area occupied by the points from each branch within a series of annuli with a fixed width of 0.5 kpc starting from the galaxy center. Interestingly, we find this ratio to persist at roughly a constant on either side of a radius of ~ 2 kpc, but abruptly switch their roles at this radius (Figure 4). Specifically, in terms of the mean values and standard deviations, we find

$$\left\langle \frac{\text{Area}_{\text{uniform mixture}}}{\text{Area}_{\text{foreground screen}}} \right\rangle = \begin{cases} 1.57 \pm 0.34 & (\lesssim 2 \text{ kpc}); \\ 0.51 \pm 0.18 & (> 2 \text{ kpc}). \end{cases} \quad (1)$$

Hence, we conclude that in the central region of M83 within a galactocentric distance of ~ 2 kpc, 61% of the nebular-emitting area follows the dust extinction properties of model 5 (uniform mixture). Beyond this radius, 66% of the nebular-emitting area follows the foreground screen model. This result is particularly useful for pixel-based statistical analyses of spiral galaxies with properties similar to M83, for which we suggest that models 5 (1) be used with a weight of $\sim 1/3$ ($2/3$) for the center and $\sim 2/3$ ($1/3$) for the outer disk. Even a more crude prescription — emitters and absorbers are assumed to be uniformly mixed in the center ($\lesssim 2$ kpc) and the foreground dust screen is employed for the outer disk — will

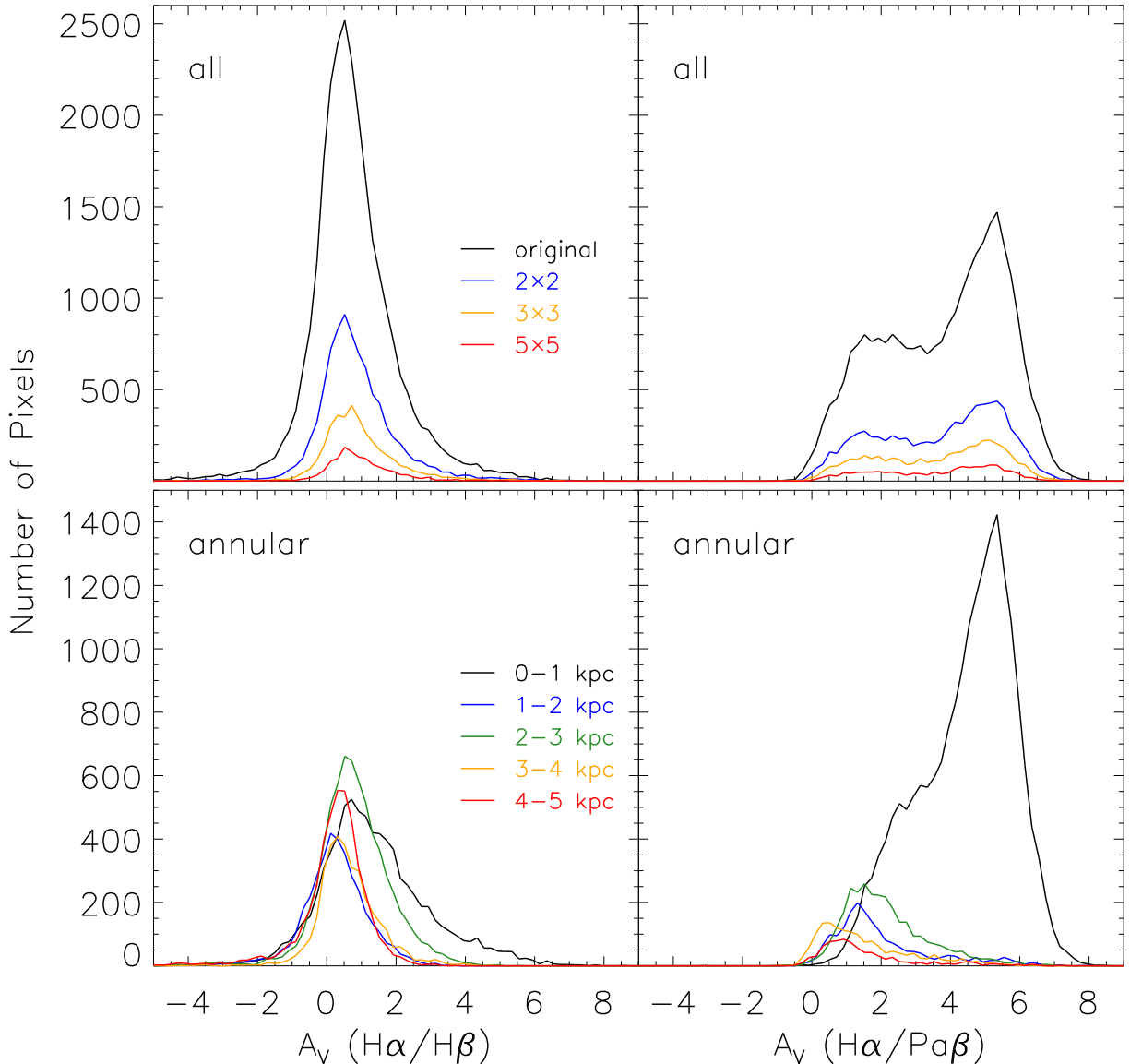


Figure 3. Histograms of the visual extinction A_V in the whole FoV (top) and a series of annuli (bottom), derived from the $H\alpha/H\beta$ and $H\alpha/P\alpha\beta$ line ratios. The difference in the number of the involved pixels is a result of their respective 5- σ cutoffs and FoVs. The histograms as a result of rebinning the maps onto a coarser grid are over-plotted in the top panels.

significantly improve the accuracy of dust extinction correction.

5. SUMMARY

As part of the Early Release Science observations made by the HST/WFC3 Scientific Oversight Committee, the starburst galaxy M83 has been imaged in multiple narrow bands targeting three hydrogen recombination lines ($H\beta$, $H\alpha$ and $P\alpha\beta$). These data enable us to scrutinize the extinction values and geometry in the H II regions by deriving the A_V map using two combinations of hydrogen lines: $H\alpha/H\beta$ and $H\alpha/P\alpha\beta$. The pixel-by-pixel comparison between the two extinction maps shows that larger optical depths are probed by the longer wavelength line emission, yielding A_V values that are larger by $\gtrsim 1$ mag than those derived from shorter-wavelength hydrogen lines. This produces a factor $\gtrsim 2$ discrepancy in the intrinsic $H\alpha$ luminosity when using the different line ratios for the extinction correction. By compar-

ing these observations to a series of simple models, we conclude that the data require a large diversity of absorber/emitter geometric configurations, but when averaged over large ($\gtrsim 100$ – 200 pc) sub-galactic regions, the mean extinction becomes consistent with the foreground dust screen model, suggesting that other geometries tend to be restricted to more local scales. Moreover, we can provide a simple prescription for improving the extinction corrections in spatially-resolved analyses, by expressing the correction in terms of two extreme geometrical dust configurations: (1) foreground non-scattering dust screen; and (2) uniform mixture of emitters and absorbers. These two configurations can be combined in the following proportions: $\sim 2/3$ ($1/3$) for uniform mixture (foreground screen) in the central area ($\lesssim 2$ kpc) and $\sim 1/3$ ($2/3$) in the outer disk.

This paper is based on Early Release Science observations made by the WFC3 Science Oversight Committee.

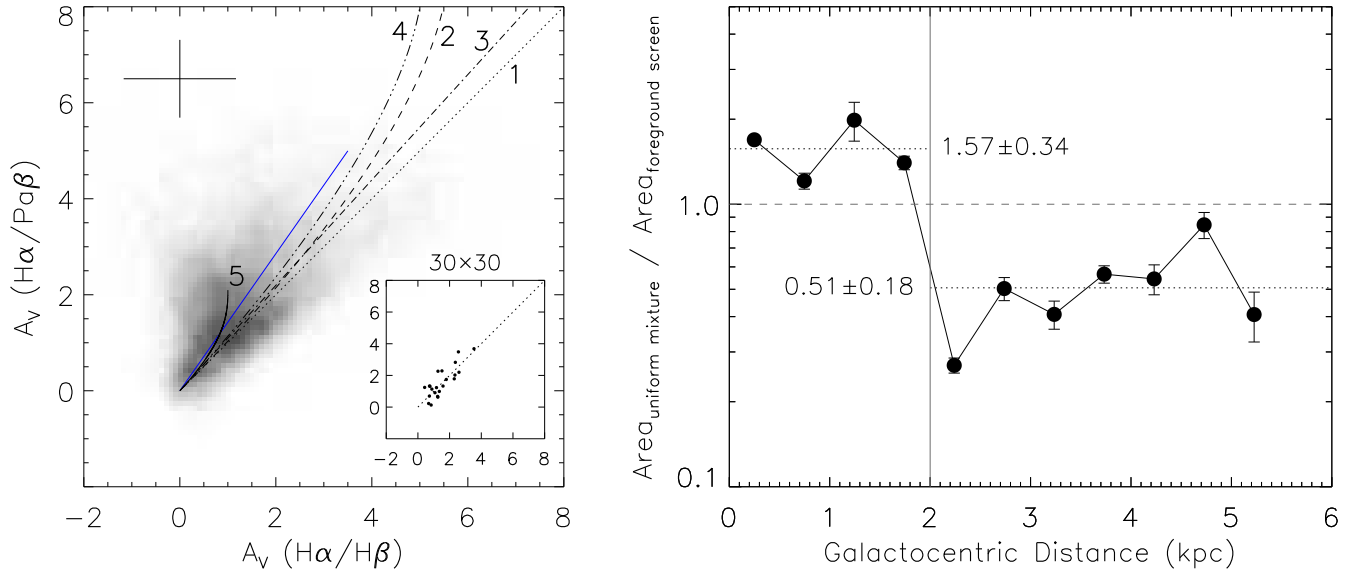


Figure 4. *Left.* The relation between A_V derived in two ways, compared to the 5 simple models discussed in the text, numbered in the same fashion (1 – foreground screen; 2 – clumpy dust screen; 3 – uniform scattering slab; 4 – clumpy scattering slab; 5 – uniform mixture). Only pixels with $S/N \geq 5$ detection in all three lines are used, and the typical $1-\sigma$ uncertainty is shown at the corner. The blue line $A_V(\text{H}\alpha/\text{P}\alpha\beta) = 1.428 A_V(\text{H}\alpha/\text{H}\beta)$ bisects the data points and approximately separates the two branches which roughly follow either model 5 or the degenerate trend of the other four models. When averaged over ~ 180 pc (i.e., a 30×30 grid), all data points become consistent with model 1. *Right.* The ratio of the area occupied by the “uniform mixture branch” to that by the “foreground screen branch” as a function of the galactocentric distance. The central region within ~ 2 kpc is dominated by “uniform mixture” pixels (61%) and thus favors model 5, while the rest of the disk is dominated by “foreground screen” pixels (66%) and favors model 1 better.

Support for program GO–11360 was provided by NASA through a grant from Space Telescope Science Institute, which is operated by the Association of Universities for Research in Astronomy, Inc., under NASA contract NAS 5-26555. We are grateful to the Director of STScI for awarding Directors Discretionary Time for this program.

Facilities: HST (WFC3).

REFERENCES

- Bresolin, F., & Kennicutt, R. C., Jr. 2002, *ApJ*, 572, 838
 Calzetti, D., Kinney, A. L., & Storchi-Bergmann, T. 1994, *ApJ*, 429, 582
 Cardelli, J. A., Clayton, G. C., & Mathis, J. S. 1989, *ApJ*, 345, 245
 Chandar, R., et al. 2010, *ApJ*, 719, 966
 de Vaucouleurs, G., de Vaucouleurs, A., Corwin, H. G., Buta, R. J., Paturel, G., Fouque, P., 1991, *Third Reference Catalogue of Bright Galaxies*, Springer-Verlag, Berlin, Heidelberg, New York
 Dopita, M. A., & Sutherland, R. S. 2003, *Astrophysics of the diffuse universe*, Berlin, New York: Springer, 2003
 Draine, B. T., Dale, D. A., Bendo, G., et al. 2007, *ApJ*, 663, 866
 Draine, B. T. 2011, *Physics of the Interstellar and Intergalactic Medium*, Princeton, New Jersey: Princeton Univ. Press, 2011
 Fruchter, A., et al. 2009, *The MultiDrizzle Handbook*, Version 3.0 (Baltimore, MD: STScI)
 Foyle, K., Wilson, C. D., Mentuch, E., et al. 2012, *MNRAS*, 421, 2917
 Galametz, M., Madden, S. C., Galliano, F., et al. 2011, *A&A*, 532, A56
 Hong, S., Calzetti, D., Gallagher, J. S., III, et al. 2013, *ApJ*, in press (arXiv:1309.0520)
 Israel, F. P., & Kennicutt, R. C. 1980, *Astrophys. Lett.*, 21, 1
 Kennicutt, R. C., Jr., Hao, C.-N., Calzetti, D., et al. 2009, *ApJ*, 703, 1672
 Knapen, J. H., Sharp, R. G., Ryder, S. D., et al. 2010, *MNRAS*, 408, 797
 Koribalski, B. S., Staveley-Smith, L., Kilborn, V. A., et al. 2004, *AJ*, 128, 16
 Liu, G., Calzetti, D., Yun, M. S., et al. 2010, *AJ*, 139, 1190
 Mutchler, M. 2010, in *Space Telescope Science Institute Calibration Workshop Hubble after SM4, Preparing JWST*, ed. S. Deustua & C. Oliveira (Baltimore, MD: Space Telescope Science Institute), 69 (<http://www.stsci.edu/institute/conference/cal10/proceedings>)
 Natta, A., & Panagia, N. 1984, *ApJ*, 287, 228
 Osterbrock, D.E. & Ferland, G.J. 2006, *Astrophysics of Gaseous Nebulae and Active Galactic Nuclei*, 2nd. ed. (Sausalito, CA: Univ. Science Books)
 Skillman, E. D., & Israel, F. P. 1988, *A&A*, 203, 226
 Thatte, N., Tecza, M., & Genzel, R. 2000, *A&A*, 364, L47
 Witt, A. N., & Gordon, K. D. 2000, *ApJ*, 528, 799